KFUPM
Journal of Undergraduate Research International

Diamond Open Access 90

Article Geosciences

The Role of Fluid Chemistry in the Diagenetic Alteration of Glauconitic Greensands: Insights from Hydrothermal Experiments

Ayah Al Aradi and Anas Muhammad Salisu*

Cite https://doi.org/10.64589/juri/231580

Submitted: April 26, 2026 Revised: May 11, 2026 Accepted: May 13, 2026

ABSTRACT

Greensands are important components of many shallow-marine sandstone successions and can strongly influence reservoir quality during burial diagenesis. However, the effects of fluid chemistry on greensand alteration and the resulting clay and cement products remain difficult to isolate in natural systems. This study addresses this issue through a simplified investigation of glauconitic sediment from the Arnager Greensand Formation, Bornholm, Denmark, focusing on hydrothermal experiments conducted at 250 °C. Four contrasting fluids were compared: natural Red Sea water, a synthetic alkaline sodium carbonate solution, $MgCl_2$-rich brine, and natural estuarine water. The starting sediment was quartz-rich and contained K-feldspar and calcite, and its clay fraction was dominated by glauconite. After 14 days of reaction, the four fluids produced distinct alteration pathways. Petrographic and geochemical analyses revealed that the Red Sea water and estuarine water promoted glauconite alteration through a smectite intermediate toward illite-rich assemblages, consistent with K-supported clay diagenesis. The $MgCl_2$-rich brine produced abundant chlorite, indicating that high Mg availability could redirect the reaction pathway toward Mg-bearing phyllosilicates. In contrast, the alkaline sodium carbonate system favored the formation of zeolite and halite, suggesting that high pH and high Na concentration induced a cementation-dominated pathway rather than an illite- or chlorite-dominated clay pathway. These results demonstrate that, at a constant temperature, fluid chemistry is the main factor controlling the direction of glauconitic greensand alteration, leading to secondary minerals with distinct porosity, permeability, and reservoir quality. This study provides an experimental framework for understanding the influence of formation-water composition on diagenetic evolution in glauconitic sandstone reservoirs.

Keywords: fluid chemistry, glauconite, hydrothermal experiment, illite, chlorite, zeolite, reservoir quality

1. INTRODUCTION

Glauconitic greensands are widespread in marine sedimentary systems and commonly associated with economically important reservoirs [1,2]. A key component of these sediments is glauconite, an iron- and potassium-rich authigenic clay mineral formed under specific environmental conditions [3]. Its occurrence is typically linked to low sedimentation rates, prolonged interactions with seawater, and fluctuating redox conditions that allow the coexistence of ferrous and ferric iron [4,5]. Therefore, glauconite serves as a useful indicator of the depositional environment and early diagenetic processes in shallow marine settings [2]. However, the significance of glauconite extends beyond depositional interpretation as it continues to evolve during burial, which can exert a strong influence on the diagenetic history and petrophysical properties of its host sandstones [6,7].

In subsurface environments, glauconite undergoes progressive diagenetic transformation driven by fluid–rock interactions [4,7]. These reactions include dissolution, cation exchange, and precipitation of secondary minerals such as smectite, illite, chlorite, and zeolites [8]. The nature of these transformation pathways has important implications for reservoir quality, as they can either enhance or degrade porosity and permeability [9,10]. For example, the dissolution of unstable phases may generate secondary porosity, whereas the precipitation of authigenic clays and cement can reduce pore connectivity and restrict fluid flow. Therefore, understanding the conditions controlling glauconite alteration is essential for predicting the evolution of reservoir properties in glauconitic sandstones.

Despite extensive research on glauconite-bearing systems [8–12], isolating the specific roles of individual physicochemical parameters remains challenging in natural settings. In subsurface environments, variables such as temperature, pH, salinity, and fluid composition often vary simultaneously, making it difficult to disentangle their relative contributions to mineral transformation. Among these factors, fluid chemistry plays a particularly important role because it directly governs mineral solubility, ion availability, and the stability of secondary phases. Variations in the concentrations of major elements, such as sodium, potassium, magnesium, and iron, can significantly affect the mineral assemblages formed during diagenesis and the rate of transformation. Therefore, controlled experimental approaches are required to focus on the influence of fluid chemistry on glauconite alteration.

Published under an exclusive license by KFUPM

In this study, we explored the role of fluid chemistry in controlling the diagenetic alterations of glauconitic greensand under hydrothermal conditions. Four contrasting fluid systems were investigated: natural seawater, an alkaline sodium carbonate solution, a magnesium-rich chloride brine, and estuarine water. These fluids were selected to represent a range of chemical environments differing in pH, salinity, and dominant cation composition. The aim of this study is to evaluate how variations in fluid chemistry influence the transformation pathways of glauconite and the formation of secondary minerals under comparable thermal conditions. By comparing the mineralogical and geochemical outcomes of these experiments, this study aims to identify the key controls governing the diagenetic reactions in glauconitic sand. These results provide new insights into fluid-driven mineral transformation processes and pave the way for accurate predictions of reservoir quality evolution in subsurface glauconitic systems.

2. MATERIALS AND METHODS

2.1. Background of the Glauconitic Greensand Used in the Study. The sediments used in this study were collected from the Upper Cretaceous (Lower–Middle Cenomanian) Arnager Greensand Formation, which is exposed along the southern coast of Bornholm, Denmark[13]. This shallow marine unit comprises a basal conglomerate with reworked Albian material that grades upward into glauconite-rich, fine-grained quartz sands deposited under storm-influenced and strongly bioturbated conditions. The formation is overlain by Arnager Limestone, with a well-exposed contact showing the downward penetration of the limestone material into the greens and intense bioturbation[14]. Arnager greensand is particularly suitable for controlled laboratory experiments on glauconite alteration because it is glauconite-rich, relatively unconsolidated, and readily accessible.

2.2. Experimental Design. Hydrothermal experiments were conducted in four different reacting fluids at 250 °C for 14 days using the same glauconitic greensand starting material (Table 1). This design allows a direct comparison of the effects of fluid chemistry on glauconite alteration. The hydrothermal experiments were performed in a multiposition autoclave equipped with independently controlled stainless-steel reactors (Fig. 1) based on previously reported protocols[15]. For each experiment, 20 g of sediment was placed in a 50 μm stainless-steel mesh and loaded into a reactor vessel. Each vessel was charged with 200 mL of the designated fluid to reach a fluid–solid ratio of 10:1. The reactors were sealed, pressurized with nitrogen gas, heated to 250 °C, and maintained at this temperature for 14 days.

After the completion of the reaction, the reactor was cooled to room temperature. The solid residue was recovered, air-dried, and prepared for mineralogical and geochemical analyses. The post-reaction fluids were collected for pH and dissolved-ion measurements.

2.3. Analytical Methods. The starting material and reacted solids were characterized using thin-section petrography, scanning electron microscopy with energy-dispersive spectroscopy (SEM-EDS), bulk X-ray diffraction (XRD), clay-fraction XRD, and wavelength-dispersive X-ray fluorescence (WD-XRF). Detailed protocols for these methodologies were described in a previous study[16]. Petrography was used to describe the grain texture and identify glauconite in the starting sediment. SEM-EDS was used to observe mineral morphology, replacement textures, and secondary mineral development. Bulk XRD revealed the main mineralogical composition of the sediment before and after the reaction, whereas the dominant clay phases and alteration products were identified by clay-fraction XRD. WD-XRF was used to determine the major oxide composition before and after the reaction. Fluid chemistry was evaluated by pH measurement, ion chromatography (IC), and inductively coupled plasma–mass spectrometry (ICP-MS). Major ions, including Na, K, Mg, Ca, and Cl, were measured to track changes in solution chemistry during the experiments. Together, the solid and fluid data provided a basis for interpreting the influence of the four fluids on dissolution, element exchange, and secondary mineral precipitation.

3. RESULTS

3.1. Starting Materials. The starting greensands were quartz-rich sediments containing abundant glauconite grains. Petrographic observations showed that green glauconite grains (Gl) were distributed among the detrital framework grains (Fig. 2A-B). In the SEM image, quartz (Qtz) and K-feldspar (KF) were identified as common framework grains (Fig. 2C), and the EDS spectrum showed distinct Si and O peaks, with minor Ca signal (Fig. 2D). The bulk chemical composition determined by WDX-XRF was dominated by SiO_2 (80.4 wt.%), with additional Al_2O_3 (5.8 wt.%), Fe_2O_3 (4.4 wt.%), CaO (4.4 wt.%), K_2O (2.7 wt.%), MgO (0.90 wt.%), and Na_2O (0.26 wt.%) (Table 2, Fig. 3). Bulk XRD results of the starting material confirmed that quartz was the dominant mineral phase followed by K-feldspar and calcite (Fig. 4). Although the clay mineral content was low in the bulk sediment (Table 3), clay-fraction XRD showed that it was dominated by glauconite (Table 4). An approximate external specific surface area was estimated to be ~0.01–0.02 m^2/g based on an average spherical size of 0.175 mm and a density of 2.5 g/cm^3. This estimate only represents the external surface

Table 1. *Conditions for the hydrothermal experiments*

Experiment	Sample ID	Solution (M)	Temperature (°C)	Duration (days)
1	RSW@250	Red Sea Water	250	14
2	SC@250	0.5 M NaCO2 Solution	250	14
3	MC@250	1 M $MgCl2 \cdot 6H_2O$	250	14
4	EW@250	Estuarian Water	250	14

RSW, Red Sea water; SC, sodium carbonate; MC, magnesium chlorite; EW, estuarine water.

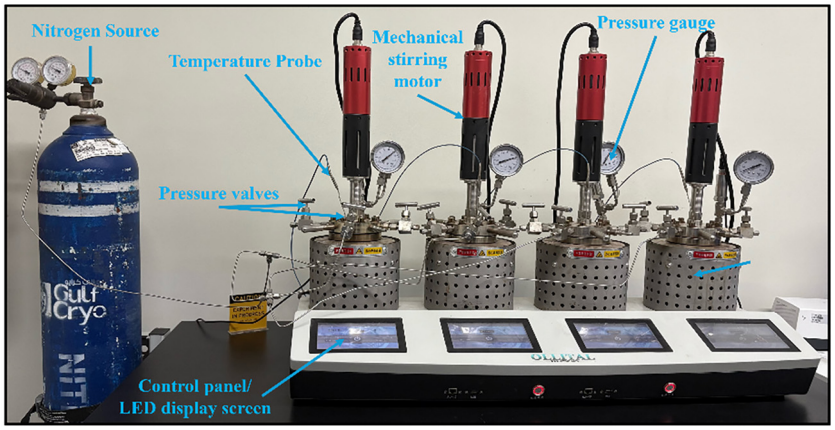


Figure 1. Hydrothermal reactor setup. The system includes four separate reactor vessels; each designed to hold up to 500 mL of solution and operate under elevated temperature and pressure conditions

and does not account for the internal porosity or clay-scale surface area typically captured by Brunauer–Emmett–Teller (BET) measurements.

3.2. Solid-Phase Geochemical Changes. The four reacting fluids induced different changes in solid-phase chemistry. In Red Sea water (Exp. 1), the reacted sediment remained silica-rich, with 79.0 wt.% SiO_2 (Table 2). CaO declined significantly relative to the starting material, suggesting calcite dissolution or the loss of carbonate components. MgO and Na_2O increased relative to the starting material, indicating an exchange between the solid and reacting fluid. Fe_2O_3 increased slightly from 4.44 wt.% to 5.64 wt.% (Table 2).

The solid after the sodium carbonate experiment (Exp. 2) also preserved a silica-rich bulk composition; however, the Na_2O content increased from 0.16 to 5.6 wt.% (Table 2), as the reaction occurred in a Na-rich alkaline fluid. Compared with the starting material, K_2O decreased from 2.7 to 1.8 wt.%, and Fe_2O_3 decreased to 3.7 wt.%. The $MgCl_2$ experiments (Exp. 3) produced the most extreme changes in the bulk chemistry of the solid. SiO_2 decreased sharply from 80.4 to 24.3 wt.%, Fe_2O_3 increased from 4.4 to 18.4 wt.%, and MgO increased from 0.9 to 8.8 wt.% (Table 2). Estuarine water experiments (Exp. 4) also induced significant chemical modification, with SiO_2 decreasing to 48.5 wt.%, while Al_2O_3, Fe_2O_3, K_2O, MgO, and Na_2O increased relative to the starting material (Table 2).

3.3. Bulk Mineralogical Changes. Bulk XRD results showed that quartz remained the dominant phase in all four post-reaction samples (Fig. 4, Table 3); however, the secondary mineral products differed depending on the fluid. In Exp. 1 (RSW), quartz increased from 79% to 87%, whereas K-feldspar decreased from 10% to 5 %, and calcite decreased from 5% to 1%. The total clay minerals increased from 2% to 4%, indicating clay-mineral development during the reaction (Fig. 5). The decrease in K-feldspar and calcite suggests that their dissolution contributed to fluid evolution and secondary mineral formation.

In the post-reaction sample from the Na_2CO_3 solution experiment (Exp. 2), quartz remained abundant at 75.4%, and the K-feldspar, calcite, and muscovite contents decreased substantially compared with the starting material (Table 3). The formation of zeolite (17.2%) and halite (3.7%) indicated that the alkaline Na-carbonate fluid induced a cementation pathway, which was different from the clay-dominated pathways observed in the natural- and Mg-rich systems (Fig. 5). In the sample from the magnesium chlorite experiment (Exp. 3), quartz remained high at 78.0%, calcite decreased from 5.3% to 0.4%, and muscovite increased from 4.1% to 13.4 % (Table 3). For the sample after the estuarine water experiment (Exp. 4), quartz remained high at 79 %, while K-feldspar decreased to 5.8%, calcite decreased to 0.1%, and muscovite increased significantly to 14.3% (Fig. 4, Table 3).

Intergranular porosity measured from thin sections decreased from 35.6% in the starting material to 27.2% (Red Sea water), 31.4% (estuarine water), 26.6% (Na2CO3 solution), and 21.2% (Mg-rich brine) (Table 3). The greatest reduction occurred in the Mg-rich brine system, whereas the estuarine water system retained comparatively higher porosity (Table 3).

3.4. Clay-Mineral Transformations. The clay-fraction XRD provided clear evidence of glauconite alteration (Table 4).

Table 2. *WDX-XRF analysis of the starting material and post-reacted samples*

		Oxides Measured in Weight Percent (wt%)									
Exp	**Sample ID**	**SiO_2**	**Al_2O_3**	**Fe_2O_3**	**CaO**	**K_2O**	**MgO**	**Na_2O**	**TiO_2**	**Cr_2O_3**	**SO_3**
SM	GS@0	80.43	5.79	4.44	4.38	2.72	0.90	0.26	0.44	0.13	0.05
Exp. 1	RSW@250	79.03	5.81	5.64	0.71	2.60	2.68	1.39	0.44	0.06	0.23
Exp. 2	SC@250	76.61	5.35	3.70	5.12	1.79	0.76	5.61	0.42	0.15	0.02
Exp. 3	MC@250	24.30	2.18	18.36	1.17	1.79	8.80	0	0.37	0.04	0.02
Exp. 4	EW@250	48.54	11.30	21.70	1.98	4.36	5.30	3.63	0.55	0.03	0.26

Exp: experiment; SM: starting material; GS: green sand; RSW: Red Sea water; SC: sodium carbonate; MC: magnesium chlorite; EW: estuarine water.

Table 3. *XRD results of the bulk and clay-fraction compositions in pre- and post-reaction samples*

	Bulk Mineralogy (%)								
Sample ID	**Qtz**	**K-fel**	**Cal**	**Mus**	**CM**	**Hal**	**Zeo**	**Total**	**Porosity**
SM	78.6	10.4	5.3	4.1	1.6	-	-	100	35.6%
RSW@250	86.8	4.9	1.1	3.2	4.0	-	-	100	27.2%
SC@250	75.4	3.1	0.1	0.5	-	3.7	17.2	100	26.6%
MC@250	78.0	8.2	0.4	13.4	-	-	0	100	21.2%
EW@250	79.8	5.8	0.1	14.3	-	-	0	100	31.4%

SM: starting material; Qtz: quartz; K-fel: K-feldspar; Cal: calcite; Mus: muscovite; CM: clay minerals; Hal: halite; Zeo: zeolite; Orth: orthoclase.

In the starting material, glauconite accounted for 95.5% of the clay fraction. After reacting with Red Sea water at 250 °C, glauconite decreased from 95.5% to 14.8%, while smectite increased from 0.8% to 27.9%, and illite became the dominant clay mineral (55.9%). In contrast, products after the $MgCl_2$ experiment exhibited 13.2% glauconite, 49.6% smectite, and 33.9% chlorite. The high chlorite content indicated that the Mg-rich fluid favored the formation of Mg-bearing phyllosilicates. The estuarine water experiment produced assemblages containing 19.2% glauconite, 37.7% smectite, and 40.6% illite. This pathway is similar to that observed in the Red Sea water experiment, where natural water promoted the evolution from glauconite to smectite and then to illite.

3.5. Fluid Chemistry After Reaction. The chemical environment of post-reaction fluids was also analyzed (Table 5 and Fig. 6). In the post-reaction Red Sea water, the pH decreased from 8.1 to 3. This strong acidification indicated substantial water-rock interactions, leading to mineral dissolution and changes in dissolved species. Fe increased significantly from 6 to 383 ppm. Meanwhile, K increased from 189 to 476 ppm (Table 5) likely due to K-feldspar dissolution, as evidenced by

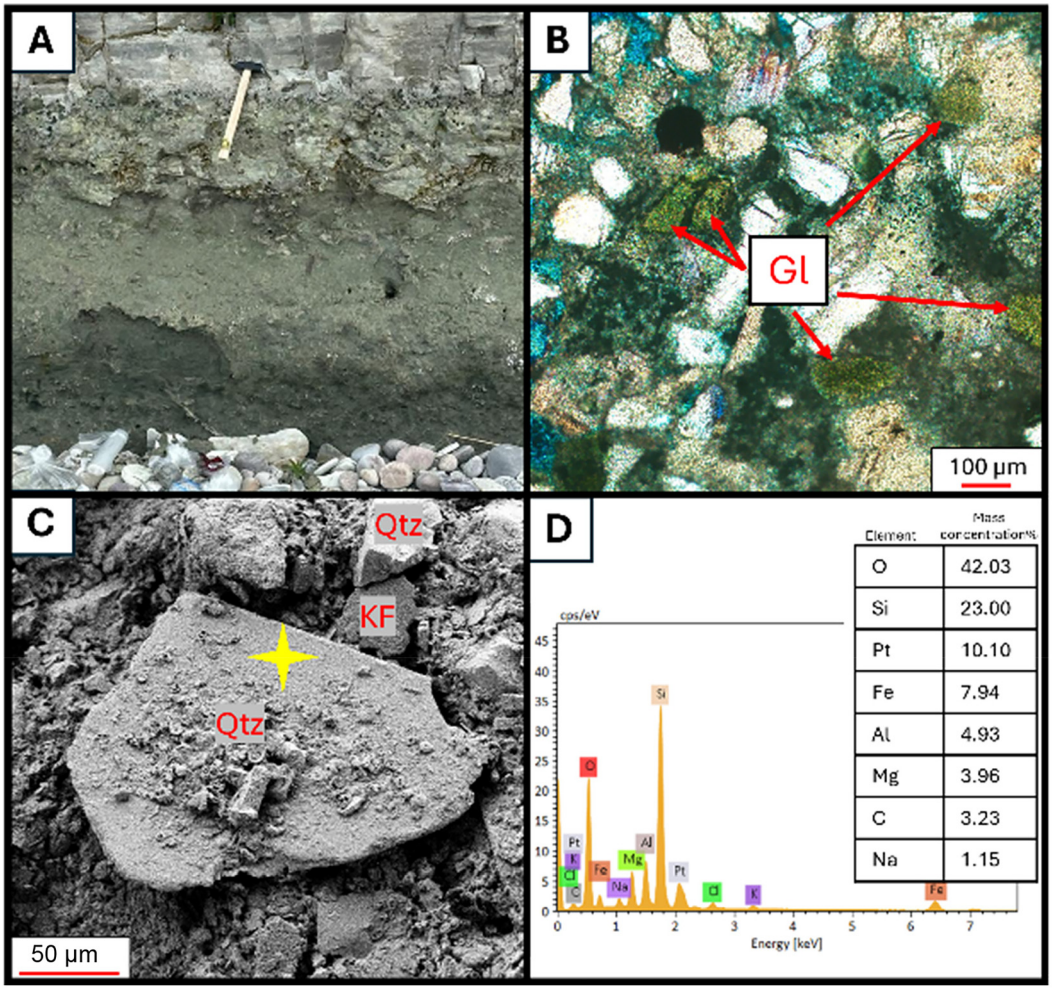


Figure 2. Characteristics of the starting material from the Arnager Greensand Formation. (A) Field image of the glauconite-bearing greensand sample. (B) Thin-section view showing glauconite-rich grains within the sediment. (C) SEM image illustrating the main mineral components of the starting material, including quartz (Qtz) and K-feldspar (KF); the yellow star indicates the location of the EDS point analysis. (D) EDS spectrum obtained from the marked spot in (C)

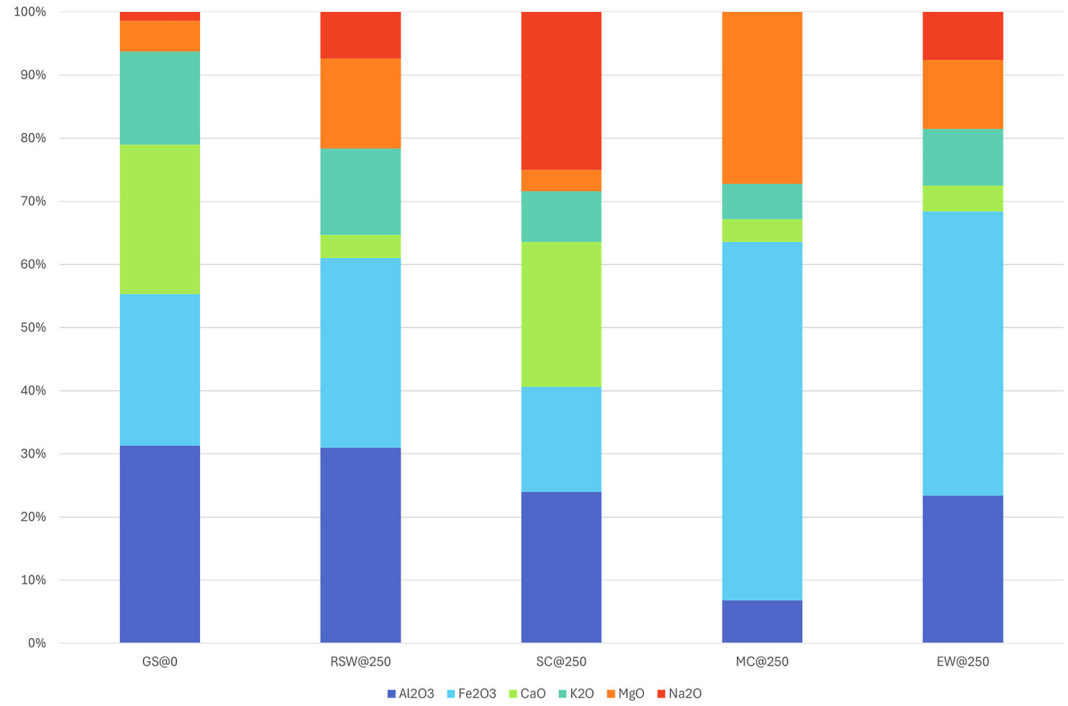


Figure 3. Stacked column plot of the WD-XRF results comparing the normalized major-oxide composition of the starting material with the reacted solids from the four 250 °C experiments. The figure shows changes in Al_2O_3, Fe_2O_3, CaO, K_2O, MgO, and Na_2O after reaction with Red Sea water, sodium carbonate solution, magnesium chloride solution, and estuarine water

the decreased K-feldspar content in the solid phase (Table 3). The increased K availability in solution can promote illite formation, which requires K as a structural component. In the sodium carbonate experiment, the fluid remained strongly alkaline with the pH decreasing only from 11.8 to 10.0. Na slightly decreased from 22,618 to 19,228 ppm, whereas K significantly increased from 48 to 709 ppm (Table 5). The high pH and elevated Na concentration facilitated the development of zeolite and halite. In the $MgCl_2$ experiment, the fluid remained acidic with the pH decreasing from 4.7 to 4.4 (Table 5). Mg increased dramatically from 13,334 to 64,623 ppm, and Cl increased from 42,700 to 251,278 ppm. This chemistry provides a strong Mg-rich environment favorable for the formation of chlorite. In the estuarine water experiment, the pH decreased from 8.2 to 5.0, while Na increased from 6981 to 19,540 ppm, and Ca increased from 283 to 2,535 ppm. Most importantly, K increased from almost undetectable to 1,351 ppm (Table 5). Combined with the observed decrease in K-feldspar in the solid phase, these changes correspond to the formation of an illite-rich clay assemblage.

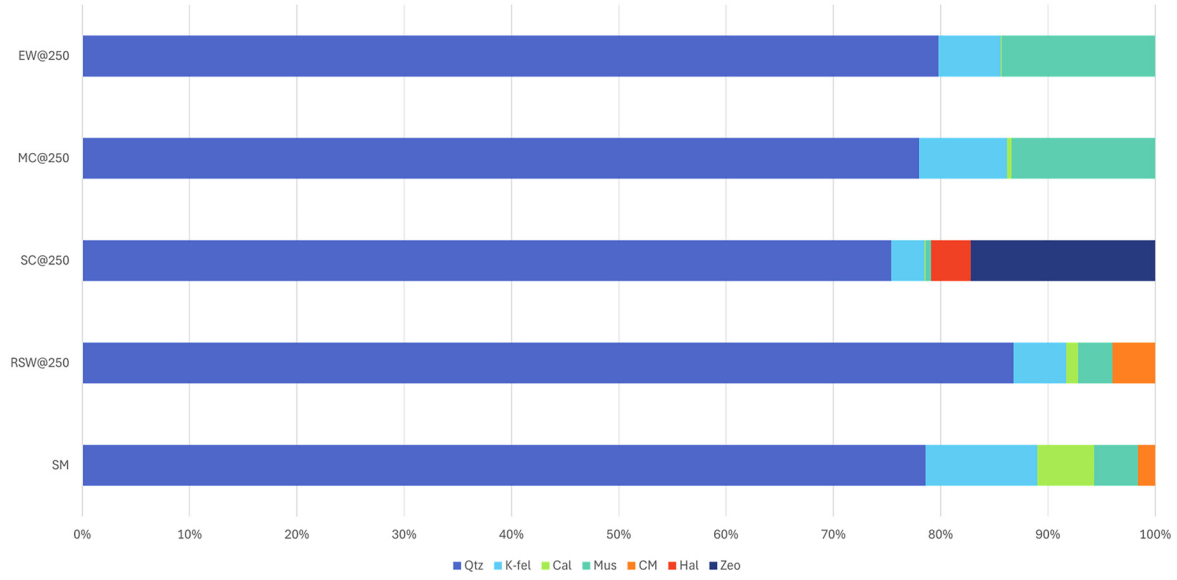


Figure 4. Stacked bar chart of bulk XRD mineralogical data for the starting material and the four reacted samples. The figure summarizes the relative proportions of the main mineral phases and highlights mineralogical differences induced by the different experimental fluids

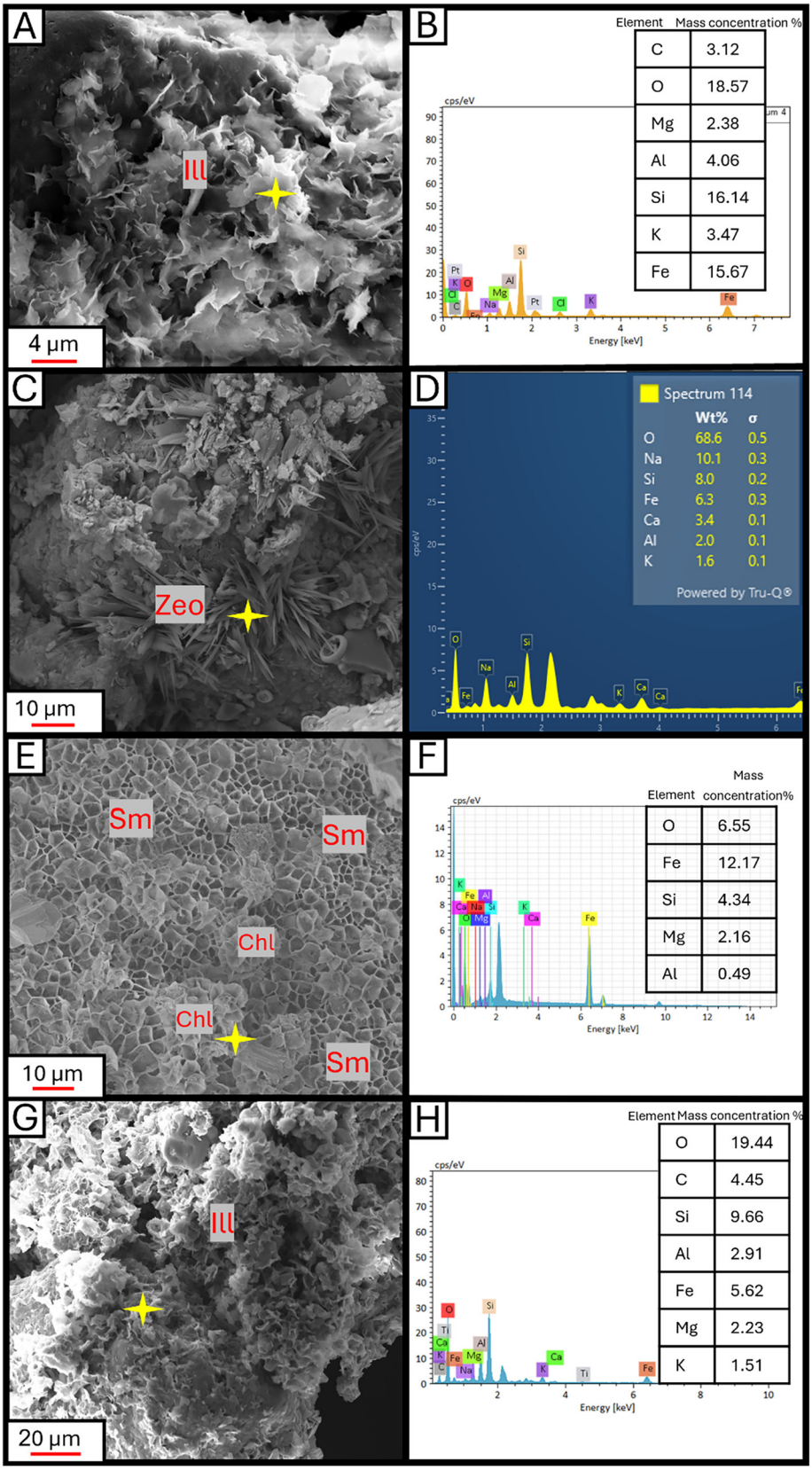


Figure 5. SEM images and corresponding EDS spectra showing mineralogical transformations in the four 250 °C hydrothermal experiments. **(A)** Red Sea water experiment showing clay-mineral development from altered glauconite, with platy to fibrous illitic/smectitic textures; the yellow star marks the EDS analysis point. **(B)** EDS spectrum from the marked area in (A). **(C)** Sodium carbonate experiment showing extensive zeolite growth associated with altered glauconite and framework grains, reflecting reaction under alkaline Na-rich conditions; the yellow star marks the analyzed spot. **(D)** EDS spectrum from the marked area in (C). **(E)** Magnesium chloride experiment showing abundant newly formed Mg-rich clay phases, including honeycomb smectite and rosette-like chlorite textures; the yellow star indicates the EDS analysis location. **(F)** EDS spectrum from the marked area in (E). **(H)** Estuarine water experiment showing glauconite alteration to smectite and further development of illitic clay textures; the yellow star marks the analyzed point. **(G)** EDS spectrum from the marked area in (H)

Table 4. *XRD clay-fraction analysis of the pre- and post-reaction samples*

	Clay Minerals (%)					
Sample ID	**Glauconite**	**Smectite**	**Illite**	**Chlorite**	**Quartz**	**Calcite**
SM	95.5	0.8	0	-	2.5	1.2
RSW@250	14.8	27.9	55.9	-	1.2	0.2
MC@250	13.2	49.6	0	33.9	2.1	1.2
EW@250	19.2	37.7	40.6	0	1.6	0.9

RSW, Red Sea water; MC, magnesium chlorite; EW, estuarine water.

4. DISCUSSION

4.1. Impact of Fluid Chemistry on Transformation Pathways of Glauconitic Greensands. The results of this study clearly demonstrate that fluid chemistry is the dominant control on glauconite alteration pathways when temperature and reaction time are held constant. Because all experiments were conducted at 250 °C for 14 d, the contrasting mineralogical outcomes can be attributed primarily to the fluid composition rather than thermal effects. Under identical thermal conditions, glauconitic greensand evolved into illite-rich assemblages in natural water (Fig. 5; Table 4), chlorite-bearing assemblages in Mg-rich brine, and zeolite-dominated assemblages in alkaline sodium carbonate solutions (Fig. 5; Table 3). These distinct pathways highlight the fundamental role of pH and key cations, particularly Na, K, Mg, and Fe, in directing diagenetic reactions. Considering that the starting materials used for the four experiments had the same external surface area (~0.01–0.02 m^2/g), the pronounced variation in mineral products across different fluid systems suggests that reaction pathways are controlled predominantly by fluid chemistry (pH and ion availability) rather than by surface-area limitations.

In all four systems, the contents of calcite and K-feldspar decreased after reaction (Table 3), accompanied by significant shifts in fluid pH and ion concentrations (Table 5) and the development of new clay minerals and cements (Table 4). These observations indicate that glauconite transformation is not a simple, single-step process but rather a dynamic system governed by dissolution, fluid evolution, and precipitation–replacement reactions. Initially, reactive components, such as glauconite, calcite, and K-feldspar, underwent dissolution or partial dissolution (Fig. 5). This was followed by the modification of fluid chemistry through the release, uptake, and exchange of dissolved ions (Table 5). Finally, secondary minerals precipitated or replaced the earlier phases once favorable saturation conditions were reached.

In natural water systems, represented by the Red Sea and estuarine waters, the dominant transformation pathway involves the evolution of glauconite toward smectite and subsequently to illite (Fig. 5, Table 4). Illite became the dominant clay mineral, reaching 55.9% in the Red Sea water experiment and 40.6% in the estuarine system, whereas smectite remained as an intermediate phase (Fig. 5, Table 4). This pattern suggests a progressive transformation pathway in which glauconite is first altered to smectite and then partially converted to illite as the reaction proceeds. Potassium availability is a key factor controlling this pathway. In both natural water experiments, K-feldspar decreased relative to the starting material, indicating its dissolution and release of potassium into the system (Table 5). This K supply is essential for illite formation [17,18]. In addition, the observed decrease in pH, particularly the strong acidification in the Red Sea water system, likely enhanced mineral dissolution and increased the availability of cations required for clay mineral growth. Together, these conditions favor the development of illite-rich assemblages. From the perspective of reservoir quality, illite commonly forms fibrous or lath-like crystals that can bridge pore throats and reduce permeability even at relatively low abundance [19–21]. Therefore, when glauconitic sandstones interact with potassium-bearing natural waters at elevated temperatures, illite precipitation may significantly reduce permeability and restrict fluid flow.

In contrast, the Mg-rich chloride brine system induces a different transformation pathway characterized by the formation of chlorite (Fig. 5, Table 4). Although glauconite was initially converted to smectite, similar to the natural-water experiments, the high magnesium concentrations redirected the reaction toward the formation of chlorite, which accounted for 33.9% of the clay fraction (Table 4). Thus, the presence of Mg ions could override potassium-driven pathways and promote the formation of Mg-rich phyllosilicates. Geochemical data, including high concentrations of dissolved Mg and increased MgO content in the solid phase, support this interpretation. The observed textures suggested a sequential pathway including the initial transformation of glauconite to smectite, followed by the partial replacement of smectite by chlorite. The impact of chlorite on the reservoir quality is more complex than that of illite. Chlorite can act as either a beneficial or detrimental phase depending on its morphology and distribution [22]. Pore-lining chlorite may inhibit quartz cementation and preserve porosity [23], whereas pore-filling chlorite tends to reduce permeability by blocking pore space [24]. In the present study, the replacement textures indicate that chlorite formation reduces pore connectivity when it develops within pore spaces or narrows pore throats as it replaces earlier phases.

A third distinctly different pathway was observed in the alkaline Na-carbonate system, where zeolite formation dominated the clay mineral development (Fig. 5, Table 3). Zeolites constituted a significant proportion of the bulk mineralogy, and their formation was accompanied by halite precipitation (Table 3). The fluid remained strongly alkaline and sodium-rich throughout the experiment, indicating that the high pH and abundant Na concentration promoted zeolite stability and precipitation. The reduced K-feldspar and muscovite contents suggested that the dissolution of aluminosilicate minerals supplied the Si and Al required for zeolite formation. Therefore, this system represents a cementation-dominated pathway that is distinct from the clay-dominated pathways observed in other experiments. The implications of this pathway for reservoir quality are significant, as zeolite cements can occupy pore spaces and reduce both porosity

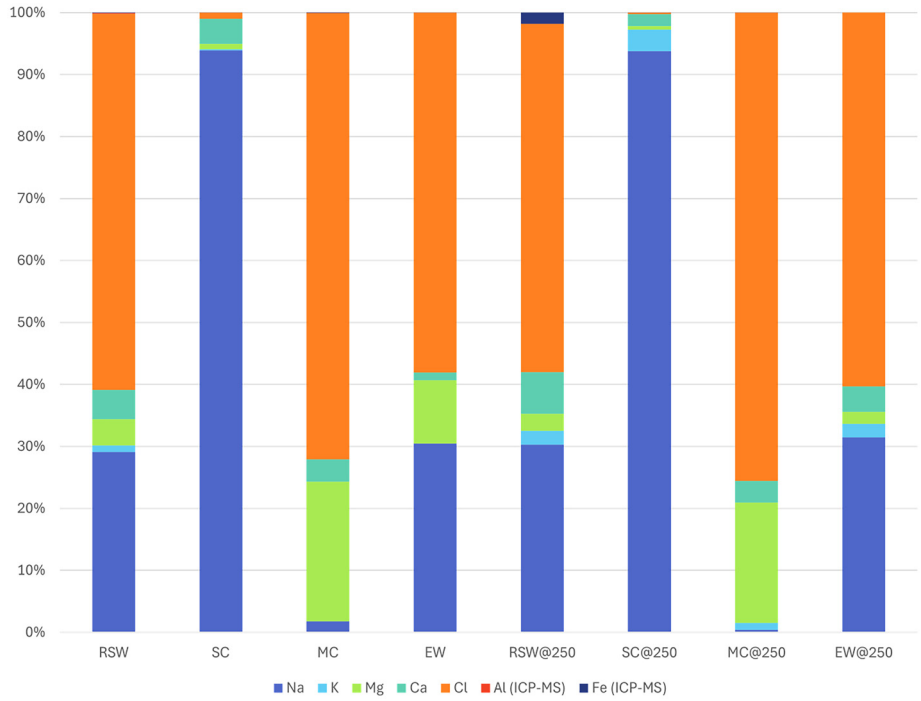


Figure 6. Fluid-chemistry bar graph based on IC/ICP-MS analyses of the initial and post-reaction solutions. The figure compares the concentrations of major dissolved components before and after reaction for each experimental fluid, including Red Sea water, sodium carbonate solution, magnesium chloride solution, and estuarine water

and permeability. However, in some geological settings, the subsequent dissolution of zeolite may generate secondary porosity[25]. In this study, the formation of zeolites under alkaline conditions suggests that Na-rich fluids pose a strong cementation risk in glauconitic sandstones, particularly when the fluids interact with reactive aluminosilicate minerals.

Collectively, the results of this study demonstrate that fluid chemistry controls the direction of glauconite transformation pathways. Variations in pH and ion availability determine whether the system evolves into illite-, chlorite-, or zeolite-dominated assemblages. These findings provide important insights into the control of diagenetic processes via fluid–mineral interactions and highlight the importance of fluid composition when predicting the evolution of reservoir quality in glauconitic sandstones.

4.2. Implications for Glauconitic Sandstone Reservoirs. This study demonstrates an important concept for reservoir prediction via simplified glauconite evolution experiments. The same glauconitic sediment can follow different diagenetic pathways depending on the formation water chemistry. Natural water, Mg-rich brine, and alkaline Na-carbonate fluid favored the formation of illite, chlorite, and zeolite, respectively. (Fig. 5; Tables 3 and 4). Each pathway has a different effect on the reservoir quality. Illite tends to reduce permeability through fibrous or lath-like pore-filling growth. Chlorite may either preserve or reduce reservoir quality, depending on whether it forms coatings or pore-filling cement[22,26]. Zeolite may act as a strong cement and reduce the porosity and permeability, although its subsequent dissolution can moderate this effect[27].

The observed porosity reduction was consistent with fluid-controlled mineral transformation pathways. The highest porosity loss in the Na-carbonate system reflects extensive zeolite and halite cementation, which likely occluded the pore space. In contrast, the porosity was largely retained in the Mg-rich system, suggesting that the formed chlorite mainly acted as a partial replacement rather than as a pervasive pore-filling cement. Natural water

Table 5. *IC analysis showing the concentration of major cations in solutions before and after the hydrothermal experiments*

		Major Cations (ppm)							
Sample ID	**pH**	**Na**	**K**	**Mg**	**Ca**	**Cl**	**Al (ICP-MS)**	**Fe (ICP-MS)**	**TDS**
RSW	8.1	5,230	189	759	847	10,908	22	6	46.0
SC	11.8	22,618	48	207	970	243	0	3	50.1
MC	4.7	1,068	-	13,334	2,139	42,700	1	18	97.1
EW	8.2	6,981	-	2,331	283	13,295	0	2	53.2
RSW@250	3.2	6,410	476	570	1,429	11,879	3	383	45.0
SC@250	10.0	19,228	709	125	388	52	0	2	40.7
MC@250	4.4	1,290	3,707	64,623	11,538	251,278	1	32	122.5
EW@250	5.0	19,540	1,351	1,224	2,535	37,487	0	1	94.2

RSW, Red Sea water; SC, sodium carbonate; MC, magnesium chlorite; EW, estuarine water.

systems show intermediate porosity losses, consistent with illite precipitation, which partially reduces pore connectivity.

These results may have strong implications for hydrocarbon reservoirs, geothermal systems, and CO_2 storage projects hosted in glauconitic sandstone. In hydrocarbon systems, clay growth and cementation can reduce producibility and increase the risk of formation damage[28]. In geothermal systems, high-temperature brine-rock reactions may cause mineral precipitation, which affects the injectivity. In CO_2 storage systems, acidification caused by dissolved CO_2 can change mineral dissolution and reprecipitation pathways, potentially affecting reservoir integrity[29]. Understanding how glauconitic greensands respond to different fluids is important for predicting their long-term reservoir behavior.

The experimental design in this study is particularly important for eliminating temperature variation and enabling a clear comparison among different fluids. The results showed that, even at the same temperature and reaction time, fluid chemistry alone can produce significantly different mineralogical outcomes. This finding supports the broader conclusion that reservoir models for glauconitic sandstones should include fluid-specific reaction pathways rather than assuming a single burial-diagenetic trend.

4.3. Limitations and Future Work. This study used controlled batch experiments, which are useful for isolating fluid chemistry but do not fully reproduce natural burial systems. Natural reservoirs are commonly open or semi-open systems in which fluids continue to move through rock, transport dissolved ions, and change saturation conditions over time. In contrast, the experiments in this study were conducted in closed systems with fixed fluid–solid ratios. The high temperature (250°C) can accelerate the reaction progress and allow for meaningful comparison among fluids; however, the 14-day duration cannot be directly converted to geological timescales.

The study on clay transformation pathways was primarily based on bulk and clay-fraction XRD characterization. Although the coexistence of smectite and illite supports a progressive transformation pathway, detailed identification of the mixed-layer illite–smectite (I–S) phases has not been undertaken. Advanced techniques such as XRD peak-profile fitting and transmission electron microscopy (TEM) can provide more precise information on the intermediate phases and reaction mechanisms, leading to a better understanding of the kinetics and structural evolution of clay minerals during diagenesis.

Future studies should include longer-duration experiments, flow-through experiments, and tests at additional temperatures to determine the kinetics of each pathway. Additional petrographic quantification of pore-filling versus pore-lining minerals is essential to improve the interpretation of reservoir-quality impacts. Finally, integrating these experimental results into reactive-transport models can predict the evolution of glauconitic reservoirs during burial, production, geothermal circulation, and CO_2 injection.

5. CONCLUSIONS

This study investigated the influence of fluid chemistry on the hydrothermal alteration of glauconitic greensands from the Arnager Greensand Formation under controlled experimental conditions (250 °C for 14 days). By comparing four chemically distinct fluid systems—Red Sea water, estuarine water, $MgCl_2$-rich brine, and alkaline sodium-carbonate solution—the experiments isolated the role of fluid composition in controlling glauconite transformation pathways and the formation of secondary minerals. The results demonstrate that fluid chemistry is a primary control on diagenetic reactions in glauconitic sandstones and significantly influences the mineralogical evolution and reservoir quality of these systems.

- At a constant temperature of 250 °C, fluid chemistry controls the alteration pathway of glauconitic greensand.
- Natural Red Sea and estuarine waters promoted glauconite alteration through smectite toward illite-rich clay assemblages, indicating a K-supported illitization pathway.
- $MgCl_2$-rich brine promotes chlorite formation, indicating that high Mg availability can redirect glauconite alteration toward Mg-bearing phyllosilicates.
- The alkaline Na-carbonate fluid favored zeolite and halite formation, indicating a cementation-dominated pathway at a high pH and elevated Na concentrations.
- Different alteration products have strong implications for reservoir quality: illite tends to reduce permeability, chlorite may either preserve or block pore systems, depending on the texture, and zeolite acts as a cement that reduces the pore space.
- These results provide a simplified framework for understanding the influences of formation water chemistry on diagenesis and reservoir quality in glauconitic sandstones.

AFFILIATIONS AND AUTHOR DETAILS

Undergraduate Author

Ayah Al Aradi – *Department of Geoscience, College of Petroleum Engineering and Geosciences, King Fahd University of Petroleum & Minerals, Dhahran 31261, Kingdom of Saudi Arabia*; 0009-0004-8645-4720
Email: s202338210@kfupm.edu.sa

Corresponding Author

Anas Muhammad Salisu – *Research Mentor, Research Scientist, Center for Integrative Petroleum Research, College of Petroleum Engineering and Geosciences, King Fahd University of Petroleum & Minerals, Dhahran, Saudi Arabia*; 0009-0002-6134-0511
Email: anas.salisu@kfupm.edu.sa

ACKNOWLEDGEMENTS

We sincerely acknowledge the College of Petroleum Engineering and Geosciences (CPG) at King Fahd University of Petroleum & Minerals for providing facilities and technical support for this study. We also express our appreciation to Arabian Drilling for sponsoring the geological field trips for sample collection. We are grateful to Prof. Khalid Al-Ramadan for his guidance, insightful feedback, and encouragement throughout this study. We also thank Dr. Ayman for his valuable assistance and support during this study. We extend our thanks to Shahad Darwish, Fatimah

Al-Ibrahim, Ayah Al-Khalifah, and Fatima Al Shammary for their contributions to sample collection and fieldwork.

REFERENCES

(1) Fernández-Landero, S. & Fernández-Caliani, J. C. Mineralogical and Crystal-Chemical Constraints on the Glauconite-Forming Process in Neogene Sediments of the Lower Guadalquivir Basin (SW Spain). *Minerals 2021, Vol. 11, Page 578* **11**, 578 (2021).

(2) Huggett, J. M. Minerals: Glauconites and Green Clays. *Reference Module in Earth Systems and Environmental Sciences* https://doi.org/10.1016/b978-0-12-409548-9.02893-1(2013)doi:10.1016/b978-0-12-409548-9.02893-1.

(3) Rubio, B. & López-Pérez, A. E. Exploring the genesis of glauconi and verdine facies for paleoenvironmental interpretation: A review. *Sediment. Geol.* **461**, 106579 (2024).

(4) Bansal, U., Banerjee, S., Ruidas, D. K. & Pande, K. Origin and geochemical characterization of the glauconites in the Upper Cretaceous Lameta Formation, Narmada Basin, central India. *Journal of Palaeogeography* **7**, 99–116 (2018).

(5) ODIN, G. S. & MATTER, A. De glauconiarum origine. *Sedimentology* **28**, 611–641 (1981).

(6) Baldermann, A. *et al.* The role of Fe on the formation and diagenesis of interstratified glauconite-smectite and illite-smectite: A case study of Lower Cretaceous shallow-water carbonates. *Chem. Geol.* **453**, 21–34 (2017).

(7) Yang, X. F. *et al.* Reservoir characteristics and hydrocarbon accumulation of the glauconitic sandstone in the Tarapoa Block, Oriente Basin, Ecuador. *J. Pet. Sci. Eng.* **173**, 558–568 (2019).

(8) Hegab, O. A. & Abd El-Wahed, A. G. Origin of the glauconite from the Middle Eocene, Qarara Formation, Egypt. *Journal of African Earth Sciences* **123**, 21–28 (2016).

(9) Diaz, E., Prasad, M., Mavko, G. & Dvorkin, J. Effect of glauconite on the elastic properties, porosity, and permeability of reservoir rocks. *The Leading Edge* **22**, 42–45 (2003).

(10) Tribovillard, N. *et al.* The contrasting origins of glauconite in the shallow marine environment highlight this mineral as a marker of paleoenvironmental conditions. *Comptes Rendus - Geoscience* **355**, (2023).

(11) Zhang, Q., Awolayo, A. N., Nightingale, M. J. & Tutolo, B. M. Kinetics of glauconite dissolution in anoxic conditions as a function of pH and temperature. *Geochim. Cosmochim. Acta* **336**, 78–91 (2022).

(12) Dasi, E., Rudmin, M. & Banerjee, S. Glauconite applications in agriculture: A review of recent advances. *Appl. Clay Sci.* **253**, (2024).

(13) Hart, M. B., Bromley, R. G. & Packer, S. R. Anatomy of the stratigraphical boundary between the Arnager Greensand and Arnager Limestone (Upper Cretaceous) on Bornholm, Denmark. *Proceedings of the Geologists' Association* **123**, 471–478 (2012).

(14) Schack Pedersen, S. A. & Gravesen, P. The geological framework for Hvideklint, south-east Denmark, using glaciodynamic sequence stratigraphy. *GEUS Bulletin* **47**, (2021).

(15) Salisu, A. M., Bello, A. M., Amao, A. O. & Al-Ramadan, K. The Role of Fluid Chemistry in the Diagenetic Transformation of Detrital Clay Minerals: Experimental Insights from Modern Estuarine Sediments. *Minerals* vol. 15 Preprint at https://doi.org/10.3390/min15030317 (2025).

(16) Bello, A. M. *et al.* Diagenetic controls on the quality of shallow marine sandstones: An example from the Cambro-Ordovician Saq Formation, central Saudi Arabia. *Journal of African Earth Sciences* **215**, 105295 (2024).

(17) Lanson, B., Sakharov, B., Claret, F. & Drits, V. Diagenetic Smectite-to-Illite Transition in Clay-Rich Sediments: A Reappraisal of X-Ray Diffraction Results Using the Multi-Specimen Method. *Am. J. Sci.* **309**, 476–516 (2009).

(18) Robinson, D., Schmidt, S. T. & De Zamora, A. S. Reaction pathways and reaction progress for the smectite-to-chlorite transformation: Evidence from hydrothermally altered metabasites. *Journal of metamorphic Geology* **20**, 167–174 (2002).

(19) Tang, L., Gluyas, J. & Jones, S. Porosity preservation due to grain coating illite/smectite: Evidence from Buchan Formation (Upper Devonian) of the Ardmore Field, UK North Sea. *Proceedings of the Geologists' Association* **129**, 202–214 (2018).

(20) Storvoll, V., Bjørlykke, K., Karlsen, D. & Saigal, G. Porosity preservation in reservoir sandstones due to grain-coating illite: A study of the Jurassic Garn Formation from the Kristin and Lavrans fields, offshore Mid-Norway. *Mar. Pet. Geol.* **19**, 767–781 (2002).

(21) Al-Ramadan, K. Illitization of Smectite in Sandstones: The Permian Unayzah Reservoir, Saudi Arabia. *Arab. J. Sci. Eng.* **39**, 407–412 (2014).

(22) Ehrenberg, S. N. Preservation of Anomalously High Porosity in Deeply Buried Sandstones by Grain-Coating Chlorite: Examples from the Norwegian Continental Shelf1. *Am. Assoc. Pet. Geol. Bull.* **77**, 1260–1286 (1993).

(23) Xia, H., Perez, E. H. & Dunn, T. L. The impact of grain-coating chlorite on the effective porosity of sandstones. *Mar. Pet. Geol.* **115**, 104237 (2020).

(24) Durand, C., Cerepi, A. & Brosse, E. Effect of Pore-Lining Chlorite on Petrophysical Properties of Low-Resistivity Sandstone Reservoir. https://doi.org/10.2118/63070-MS(2000)doi:10.2118/63070-MS.

(25) Wang, J., Zhou, L., Liu, J., Li, E. & Xian, B. Genesis of diagenetic zeolites and their impact on reservoir formation in the Middle Permian Lower-Wuerhe Formation of the Mahu Sag, Junggar Basin, Northwest China. *Energy Exploration & Exploitation* **38**, 2541–2557 (2020).

(26) Worden, R. H. *et al.* Chlorite in sandstones. *Earth. Sci. Rev.* **204**, 103105 (2020).

(27) Hay, R. L. & Sheppard, R. A. Occurrence of Zeolites in Sedimentary Rocks: An Overview. *Rev. Mineral. Geochem.* **45**, 217–234 (2001).

(28) Worden, R. & Morad, S. Clay Minerals in Sandstones: Controls on Formation, Distribution and Evolution. in *Clay Mineral Cements in Sandstones* vol. 34 1–41 (2009).

(29) Weibel, R. *et al.* Reactivity of glauconitic sandstones in CO2 experiments. *International Journal of Greenhouse Gas Control* **148**, (2025).